ELSEVIER

Contents lists available at ScienceDirect

NDT&E International

journal homepage: www.elsevier.com/locate/ndteint



Processing strategies for high-resolution GPR concrete inspections

Johannes Hugenschmidt a,*, Alexis Kalogeropoulos a, Francesco Soldovieri b, Giancarlo Prisco b

- ^a Empa, Swiss Federal Laboratories for Materials Testing and Research, Ueberlandstrasse 129, 8600 Duebendorf. Switzerland
- b IRÊA, Istituto per il Rilevamento Elettromagnetico dell'Ambiente, Consiglio Nazionale delle Ricerche, Via Diocleziano 328, 80124 Naples, Italy

ARTICLE INFO

Article history:
Received 15 September 2009
Received in revised form
1 February 2010
Accepted 28 February 2010
Available online 4 March 2010

Keywords: GPR Concrete High-resolution Data processing Inversion

ABSTRACT

A high-resolution multi-sensor and multi-polarization Ground Penetrating Radar (GPR) dataset was acquired on a concrete retaining wall. This dataset was characterised as a low pass filter with the help of a moving window spectral analysis. In order to examine the benefits and limits of innovative processing strategies, the dataset was processed with three different methods: classical 2-D processing, full 3-D processing followed by data fusion and inverse scattering followed by data fusion. A comparison of the results for two layers of rebar present in the wall shows that the innovative approaches improve the results for near surface structures when compared to classical 2-D processing. For deeper structures, the benefits of the innovative approaches are limited because of the low pass properties of the concrete.

© 2010 Elsevier Ltd. All rights reserved.

1. Introduction

In many cases, concrete structures contain a complex interior of rebar, tendons, rock anchors and/or additional fixtures. Thus, three-dimensional Ground Penetrating Radar (GPR) surveys are often a necessity to obtain a clear visualization of the interior of a structure. The acquisition of three-dimensional datasets is a demanding task that has to be carried out on objects as different as retaining walls, bridge decks or piles and requires high accuracy of positioning. In addition, the directionality and size of the acquired datasets pose a challenge in terms of data processing strategies.

Several authors have suggested acquisition and processing strategies for high-resolution GPR data acquired on concrete. Hugenschmidt and Mastrangelo [1] and Hugenschmidt and Kalogeropoulos [2] describe the acquisition and processing of pseudo 3-D data from retaining walls at a Swiss motorway by exploiting single polarized antennas. Kohl et al. [4] describe the fusion of radar data with different polarizations and the combination with ultrasonic data. Langenberg et al. [5] describe a unified theory of modeling and imaging with electromagnetic and elastic waves for the non-destructive testing of concrete. Capizzi and Cosentino [6] investigate different dipole configurations in experimental tests using longish objects in a homogeneous medium. Sbartai et al. [7] suggest the use of an

artificial neural network for solving the inverse problem related to radar data acquired on reinforced concrete. The application of an inverse scattering algorithm to radar data acquired on reinforced concrete is suggested by Soldovieri et al. [8–11]. In fact, the adoption of a linear inverse scattering approach based on a simplified model of the electromagnetic scattering permits many applicative advantages in terms of fast and effective processing. This is very suitable to perform high-resolution imaging using large datasets in quasi real time [10].

In this paper, we deal with the inspection of a retaining wall [2] by adopting an advanced data acquisition apparatus able to produce 3-D high-resolution multi-polarization datasets, thanks to the simultaneous exploitation of two antennas with different orientations. The adoption of strategies based on signal processing techniques and an inverse approach, able to exploit in an effective way the diversity in the polarization, makes it possible to map the two layers of rebar embedded in the wall.

In particular, the dataset was processed with three different approaches, classical 2-D processing, 3-D processing followed by data fusion and inverse scattering followed by data fusion. This paper presents the data acquisition and the three processing strategies together with their results. The comparison of these results for two layers of rebar leads to conclusions concerning the data acquisition and processing of high resolution GPR surveys.

Therefore, the paper is organized as follows. Section 2 is devoted to the description of the inspected wall, data acquisition and a description of the acquired dataset. In Section 3, the three processing strategies are briefly depicted by referring to 2-D reconstructions of vertical profiles. In Section 4 the performances of the proposed strategies are compared in terms of 3-D

^{*} Corresponding author. Tel.: +41 44 823 43 18.

E-mail addresses: johannes.hugenschmidt@empa.ch (J. Hugenschmidt), soldovieri.f@irea.cnr.it (F. Soldovieri).

representations by considering the top and a deeper layer of rebar. The most important conclusions are summarized in Section 5.

2. Data acquisition

Data were acquired on a retaining wall near Empa, Switzerland (Fig. 1) along vertical lines. The concrete wall (Fig. 2) increases in thickness from top to bottom and contains two layers of rebar with overlaps near the top and the bottom of the wall. Vertical bars have a nominal diameter of 0.016 m and a distance of 0.2 m between single bars. Horizontal bars have a diameter of 0.012 m and a distance of 0.15 m. In addition, there are distance pieces with a diameter of 0.014 m connecting the two layers of rebar. Only one side of the wall is accessible as the other side is hidden by ground.

The equipment used consisted of a GSSI SIR-20 radar unit, two GSSI model 5100 antennas and an acquisition apparatus developed at Empa for data acquisition on retaining walls [1,2]. The apparatus consists of a ladder like guiding system for the antenna box, a rail system sitting on the coping of the wall for lateral displacement and an electric motor for moving the antenna box up and down. The desired positioning accuracy of 0.01 m is achieved by the combination of a survey wheel controlling the vertical position, the rail system for an accurate position of the top of the apparatus and an electronic protractor system for the vertical alignment of the guiding system and thus the path of the antenna box. The centre frequency of the antennas as examined by Empa in a laboratory experiment [3] is 1.25 GHz in air. Both antennas were placed in the same antenna box, recording simultaneously. The antennas were orientated with horizontal and vertical E-fields (Fig. 3), thus permitting multi-polarization measurements.

The acquisition parameters for single antennas can be summarized as follows:

Trace length: 15 ns
Samples per trace: 512
Traces per meter: 400
Line spacing: 0.01 m

• Transmitter–receiver offset: 0.06 m

• Data processing during acquisition: none

The coordinate system used throughout this paper is presented in Fig. 4, with *X* and *Y* being parallel to the front of the wall. All data were acquired moving the antenna box along the *X*-axis from the top to the bottom of the wall. This is due to the acquisition



Fig. 1. Retaining wall with acquisition apparatus.

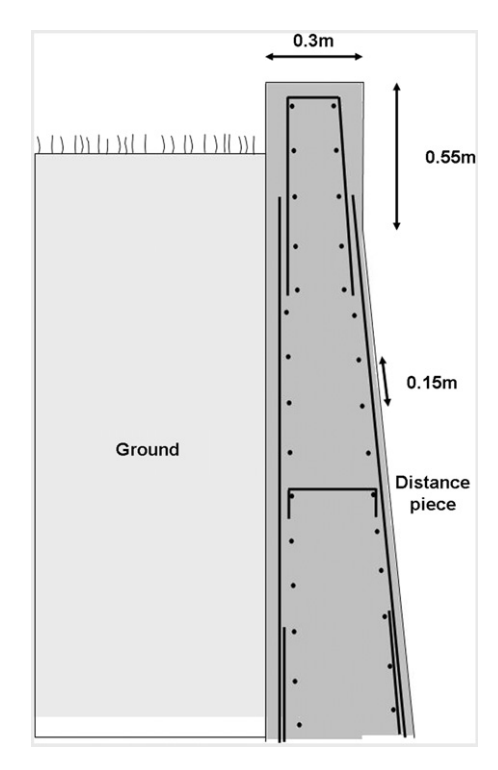


Fig. 2. Retaining wall, simplified plan compiled from several original building plans.

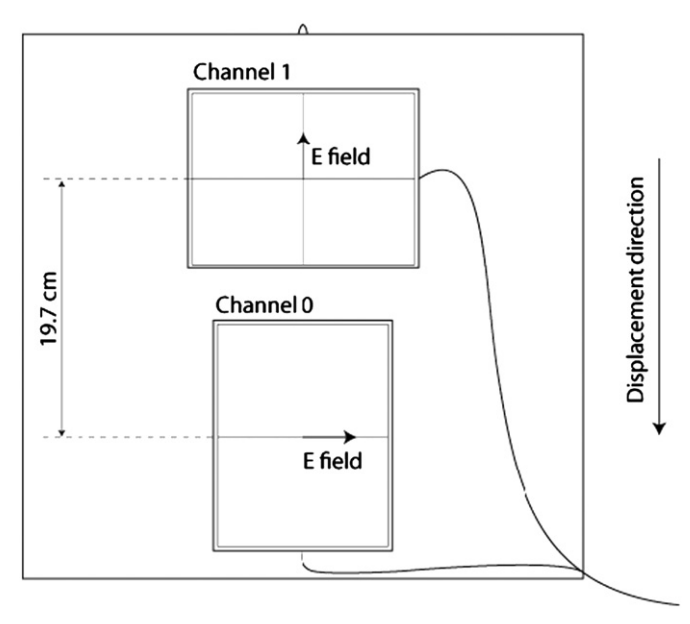


Fig. 3. Antenna box.

apparatus, which is designed for the acquisition along vertical lines parallel to the *X*-axis. The dataset acquired for this study covers 1.40 m in the *Y*-direction corresponding to 141 single lines and 2.42 m in the *X*-direction for each antenna.

A comparison between the raw datasets collected with the two antenna polarizations on the same line is presented in Figs. 5 and 6. As expected, the antenna with the horizontal *E*-field is able to detect reflections in terms of hyperbolae mainly from horizontal (parallel to the *Y*-axis) bars whereas the antenna with the vertical *E*-field maps mainly vertical (parallel to the *X*-axis) bars (arrows in Fig. 6). In order to further characterize the data, a moving window spectral analysis was applied to the two datasets shown in Figs. 5 and 6. The moving window spectral analysis computes

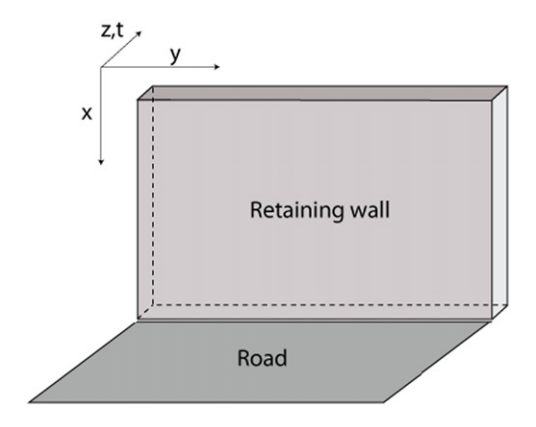


Fig. 4. Coordinate system.

amplitude spectra within time windows of a defined length via Fast-Fourier-Transform (FFT). The time window is moved along the single traces and the result of the FFT is assigned to the sample in the centre of the window. Following this the amplitude spectra of all traces are added together. Before the computation of the moving window spectrum the direct wave/surface reflection was removed from the data. A time window of 2 ns was used. The result is shown in Fig. 7 for the horizontal E-field data (left) and the vertical E-field data (right). In order to improve the comprehensibility of the figures, the sum of a range of 262 MHz was grouped together in one trace. In the spectrum of the horizontal E-field data, all frequencies shown have their maximum between 4.0 and 5 ns. This is due to the fact that this corresponds to the reflections from the top layer of rebar. Looking at the quotients of the maximum amplitudes between 9 and 12 ns divided by the maximum amplitudes between 3.8 and 4.8 ns

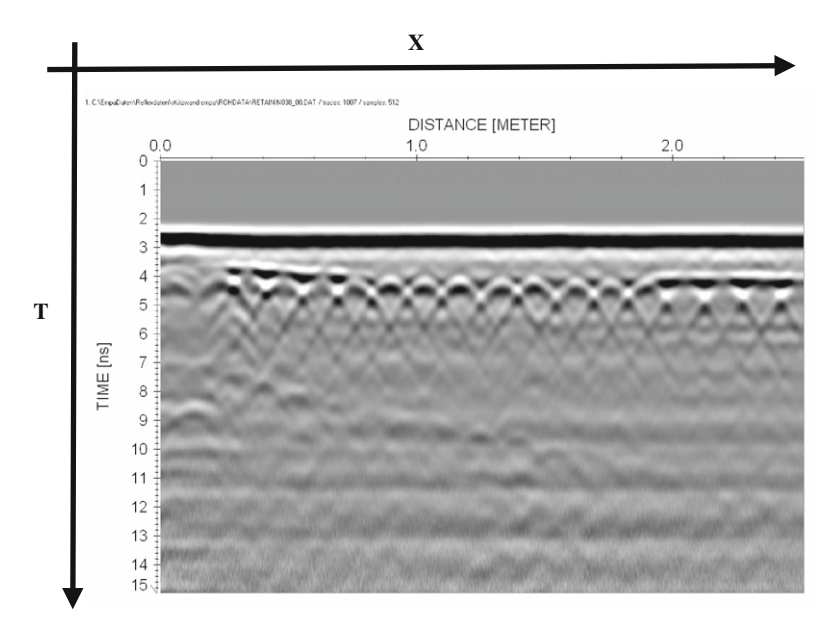


Fig. 5. Raw dataset, horizontal *E*-field, y=0.37 m.

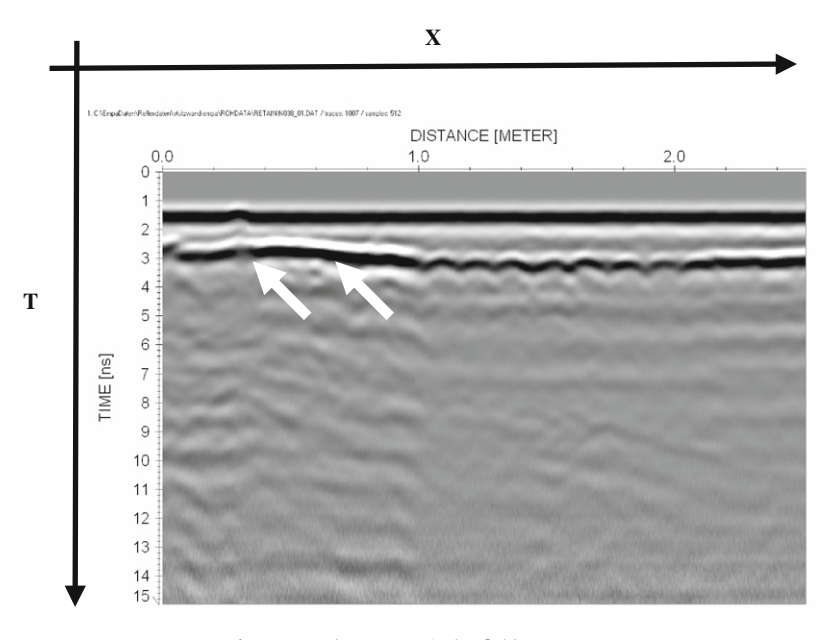


Fig. 6. Raw dataset, vertical *E*-field, y=0.37 m.

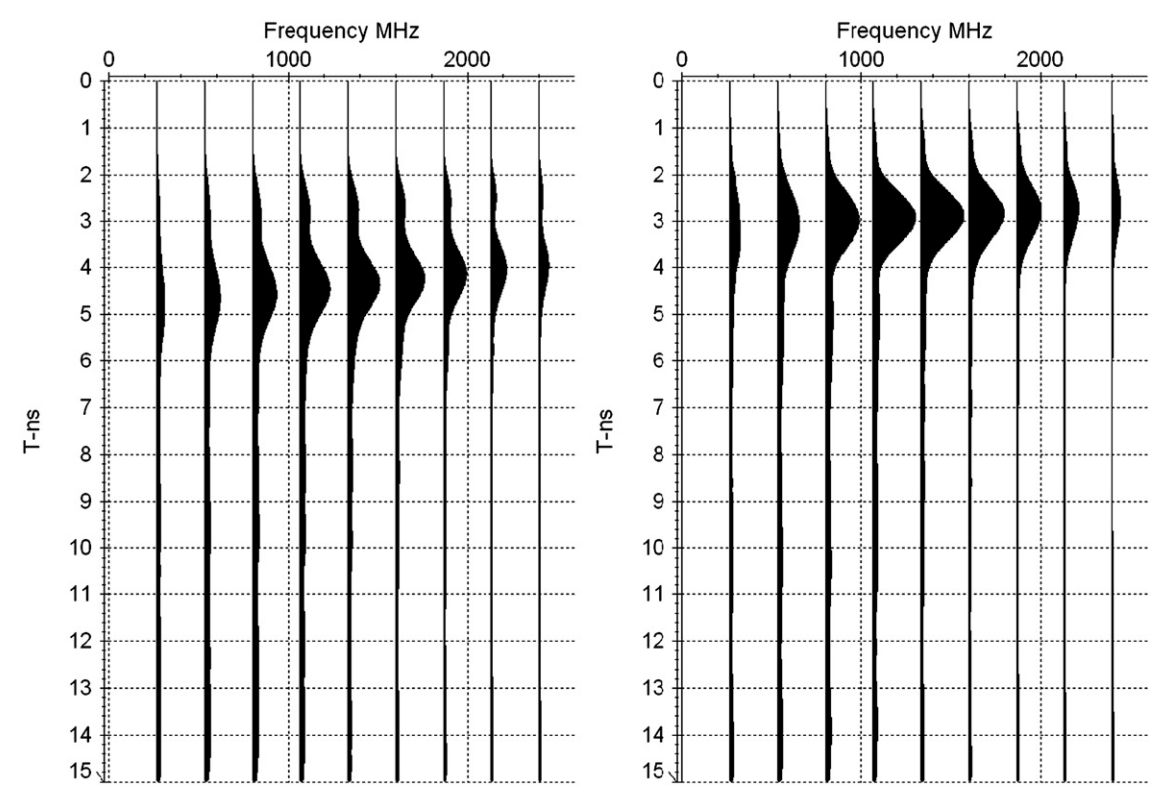


Fig. 7. Moving window spectrum, horizontal E-field (left) and vertical E-field (right), direct wave/surface reflection removed, window length 2 ns.

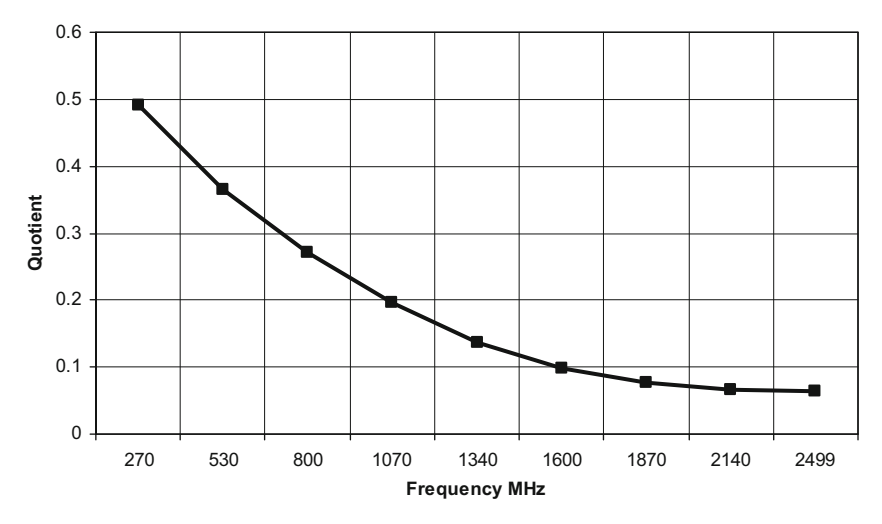


Fig. 8. Quotient of maximum amplitudes in time gates 9–12 ns/3.8–4.8 ns, horizontal *E*-field.

enables an analysis of the damping with respect to two-way travel time. The time range between 9 and 12 ns was chosen because of the presence of a second layer of rebar (see below for details). The quotient presented in Fig. 8 shows a clear decay of higher frequencies for the later time gate and gives a quantitative description of the concrete structure acting as a low pass filter.

3. Processing strategies

The raw data were processed using three different strategies:

 conventional 2-D processing using the horizontal E-field data only followed by the construction of a 3-D dataset for the presentation of the data;

- full 3-D processing of the datasets collected by the two antennas followed by data fusion during which the two datasets were combined into one dataset [2];
- inverse scattering followed by data fusion [9].

The processing following the three processing strategies was carried out independently using the optimum processing parameters for the particular strategy.

In principle, it would have been possible to apply the data fusion also for the 2-D processing. It was decided not to fuse the data processed in 2-D to demonstrate a wide span of processing options from standard to advanced strategies.

The following section is divided into three subsections that describe the three strategies and present results for the 2-D vertical profiles.

3.1. 2-D processing

The 2-D processing sequence was carried out using REFLEXW software from Sandmeier scientific software [12,13]. Only data from the antenna with the horizontal *E*-field were used and processed with the following processing sequence:

- band-pass filter applied in the frequency domain;
- correction of surface reflection/direct wave to time zero;
- Kirchhoff migration assuming a dielectric permittivity of 6.25;
- background removal;
- gain.

In addition all datasets were cut to the same length in the X-direction and time to facilitate the construction of the 3-D dataset. In Fig. 9 a vertical profile of the processed dataset corresponding to the raw data in Fig. 5 is presented. When comparing the processed data to the raw data it can be seen that the signal to noise ratio has been improved and the diffraction hyperbolae caused by the rebar running in the Y-direction (horizontal bars) have been collapsed into dots.

3.2. 3-D processing and data fusion

This processing strategy was implemented in three steps. First, 2-D processing was applied to each line acquired in the X-direction of the two datasets, then data were combined into two 3-D datasets (one for each antenna) for 3-D migration [12,13] and finally the two datasets were merged line by line. The 2-D processing was applied line by line to the datasets of both antennas using REFLEXW software. The processing sequence consisted of a time shift, a Dewow (mean subtraction) filter, gain correction, background removal, spiking-deconvolution and an F-K filter. Deconvolution was applied mainly to increase resolution. The filter was calculated using a recursive autocorrelation algorithm (Levinson) on part of the traces (0–13 ns). This filter was then convolved with the original traces with 50% white noise added

Following 2-D processing, lines were merged into the 3-D datasets separately for the two antennas. The data were migrated in 3-D using Stolt's algorithm and a signal velocity of 0.105 m/ns.

For the fusion of the two migrated datasets, three different strategies were tested. As the maximum and average algorithms described by Kohl et al. [4] did not produce satisfactory results, the datasets were decomposed into five frequency ranges with the help of a Coiflet wavelet and fused as described by Hugenschmidt and Kalogeropoulos [2]. To achieve this, each trace was decomposed into sub-spaces using finite time, oscillating, zero mean signals called wavelets [14]. Numerous wavelets types are mentioned in the literature. After testing several families of wavelets (Daubechies, Symlets, Coiflets, Haar) it was concluded that Coiflet wavelets gave the best result. This is because, according to the literature, the shape of the wavelet should be as close as possible to the shape of the emitted radar pulse [15]. Then the corresponding sub-spaces from both traces (with the different antenna orientations) were merged using the wavelet fusion algorithm, which can be considered as computing the average for the low frequency components and the maximum for the high frequency components. This was followed by the reconstruction of the fused traces using the inverse wavelet transform. In Fig. 10 the fused dataset corresponding to the raw datasets in Figs. 5 and 6 is presented.

3.3. Inverse scattering and data fusion

In order to tackle the 3-D inverse scattering problem, a 2-D slice based inversion approach [9] was applied separately to the two datasets acquired with the two antennas:

- Step 0: Preprocessing.
- Step 1: Tomographic reconstruction of the 2-D datasets.

Following steps 0 and 1, data were transferred from 2-D to 3-D.

- *Step* 2: Superimposition and interpolation of the 2-D tomographic reconstructions to obtain the 3-D representation.
- *Step* 3: The final 3-D reconstruction was obtained by fusing the two 3-D single polarization antenna results using a maximum algorithm.

During step 0, the data were prepared for the tomographic reconstruction. First, the first part of the time domain traces corresponding to direct waves and surface reflections were set to zero. Then, data were transformed to the frequency domain before the inversion algorithm was applied [8–11].

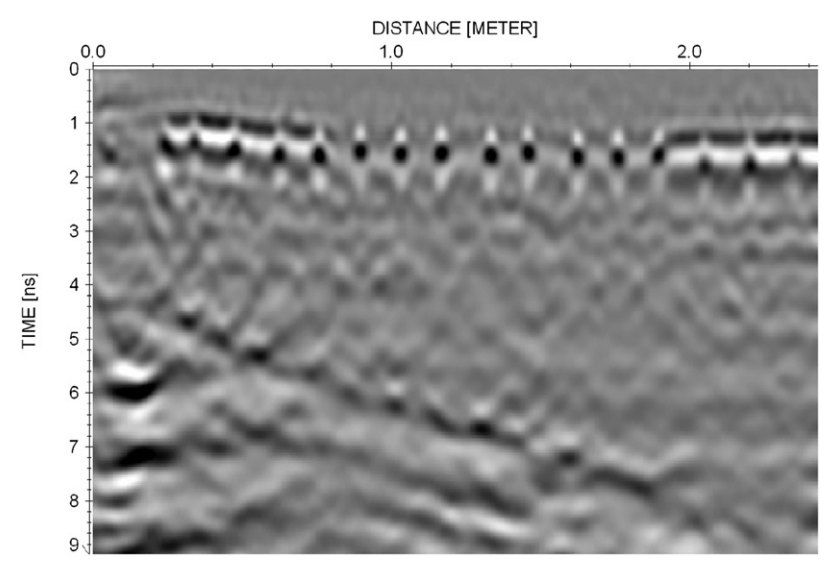


Fig. 9. Dataset after 2-D processing, horizontal *E*-field, y=0.37 m

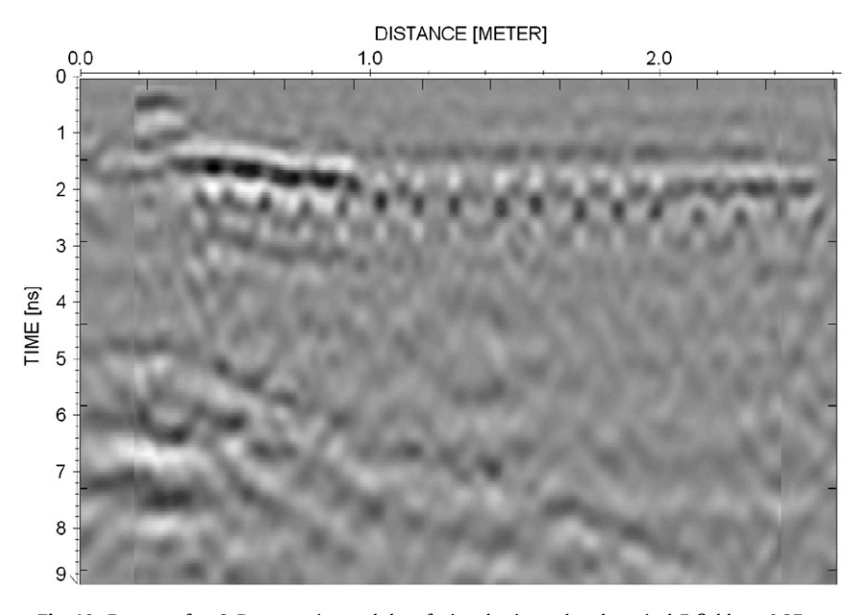


Fig. 10. Dataset after 3-D processing and data fusion, horizontal and vertical *E*-field, y=0.37 m.

During step 1, a microwave tomography based approach able to give focalized 2-D images of the rebar was applied to the two times 141 datasets. The algorithm is based on a linear model Born approximation for the electromagnetic scattering (neglecting the mutual interactions between the targets supposed invariant along the impinging/recording polarization direction) and works in the frequency domain. The result is given in terms of the modulus of the contrast function that accounts for the difference between the dielectric and conductive properties of the targets and those of the host medium (concrete hosting rebar). The regions where the modulus of the contrast function is significantly different from zero account for the presence, location and geometry of the buried targets. It is worthy noting that the adoption of a Born model inversion scheme allows one to detect, localize and determine the geometry of an object also in the case of strong scattering (for which the Born model does not hold in principle), as already shown by a large number of numerical and realistic experiments [10,11].

The parameters used for the reconstruction are listed below:

- model relative dielectric permittivity of the concrete: 9;
- model Conductivity of the concrete: 0.001 S/m;
- frequency band: 500-1500 MHz;
- frequency step: 50 MHz (21 frequencies exploited in the inversion);
- investigation domain: 1.0 m (horizontal) and 0.02-0.52 m (depth).

The fusion of the two 3-D datasets (step 3) was carried out by using the maximum value of modulus of the contrast function of the two separate 3-D reconstructed datasets. In Fig. 11, a section of the inverted and fused dataset corresponding to the raw datasets in Fig. 5 and Fig. 6 is presented.

4. 3D results

This section shows and compares the reconstruction results of the three strategies in terms of 3-D pseudo representations. In particular, the section is divided in two subsections related to the investigation of two different layers of rebar. One of those layers is at shallow depth (top layer) and a second layer is at greater and varying depth (second layer of rebar).

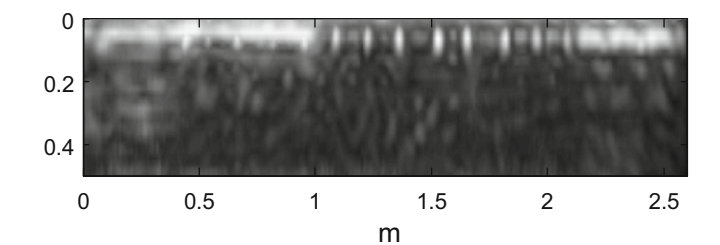


Fig. 11. Dataset after inverse scattering and data fusion, horizontal and vertical E-field, y=0.37 m.

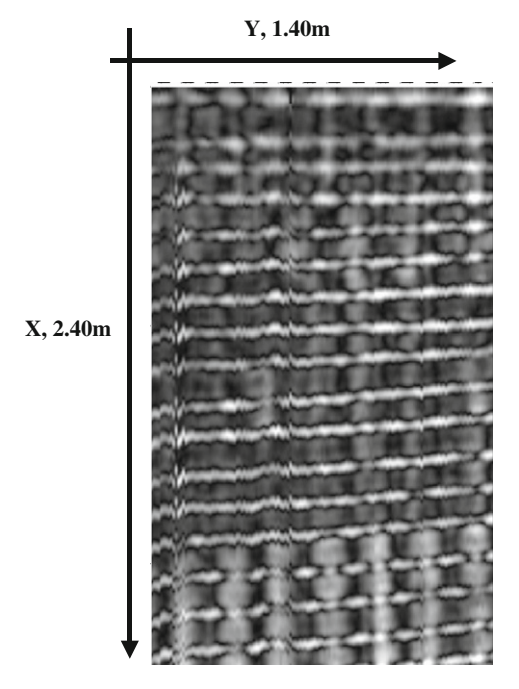


Fig. 12. time slice, t = 1.45 - 1.95 ns, 2-D processing.

4.1. Top layer of rebar

The results of the 2-D processing are presented as a time-slice and a 3-D cube in Figs. 12 and 13, respectively. The horizontal

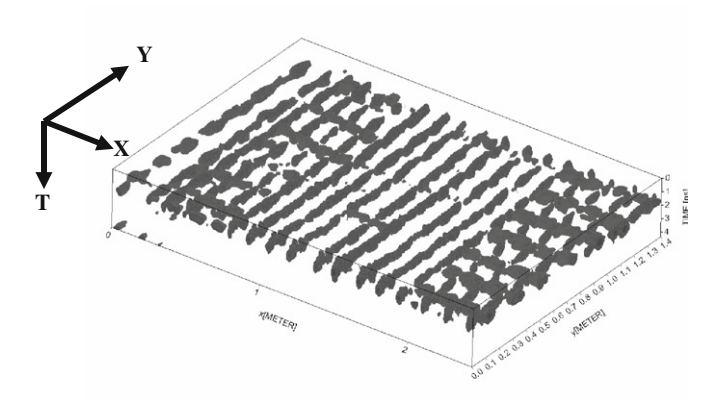


Fig. 13. Data cube 0-4 ns, 2-D processing.

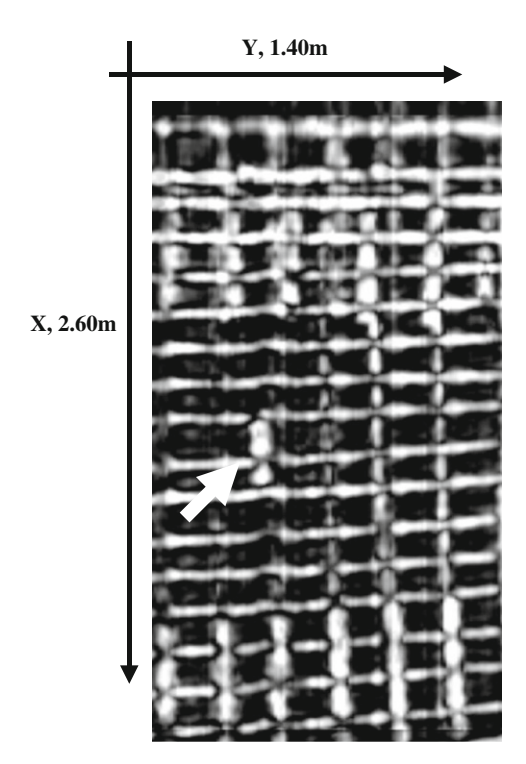


Fig. 14. time slice, t=1.45-2.08 ns, 3-D processing and data fusion.

rebar (rebar in Y-direction) is mapped reasonably whereas the vertical bars (bars in X-direction) are of low amplitude and poorly resolved. This is due to the fact that only the antenna with the horizontal *E*-field (*E*-field in Y-direction) was used and that data were migrated only in the X-direction.

In Figs. 14 and 15 the data after 3-D processing and data fusion are presented. When comparing Figs. 12–14, the most obvious difference is related to the vertical (*X*-direction) rebars, which are now mapped with a similar quality as the horizontal bars due to true three-dimensional migration and the exploitation of the multi-polarization data. In addition, increased reflection amplitudes are perceptible in the top and bottom sections of the wall and an additional reflection, most likely caused by a distance piece, becomes visible (arrow).

The combination of inverse scattering and data fusion leads to the result presented in Figs. 16 and 17. In the depth slice presentation of the dataset, the reconstruction of the vertical and horizontal bars is of the same quality and an improvement of the image quality at the top and bottom sections of the wall is

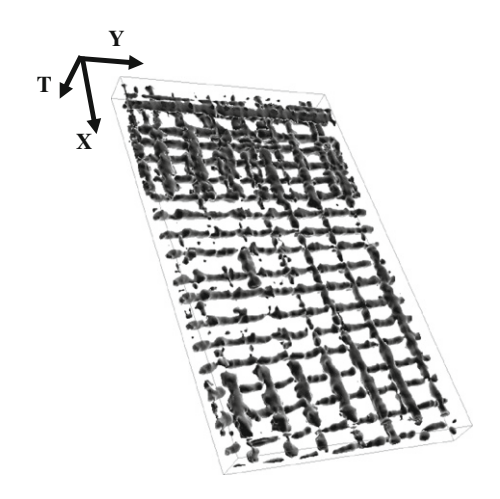


Fig. 15. Fused dataset after 3-D processing and data fusion, 0.5-3.5 ns.

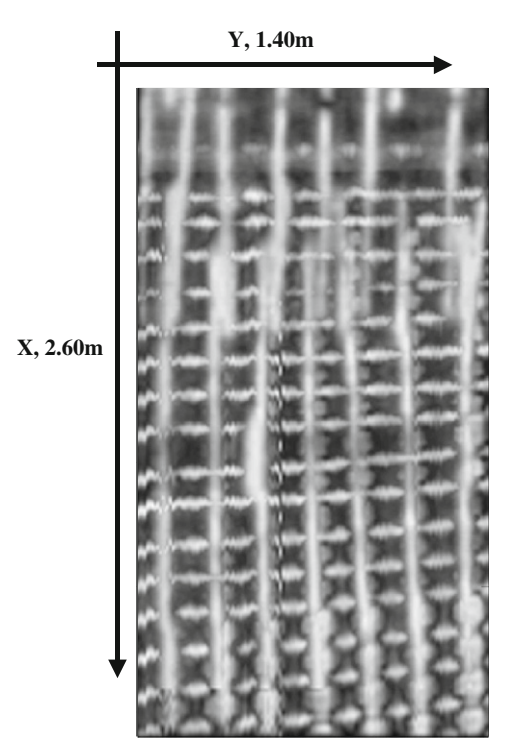


Fig. 16. Depth slice, depth=6 cm, inverse scattering and data fusion.

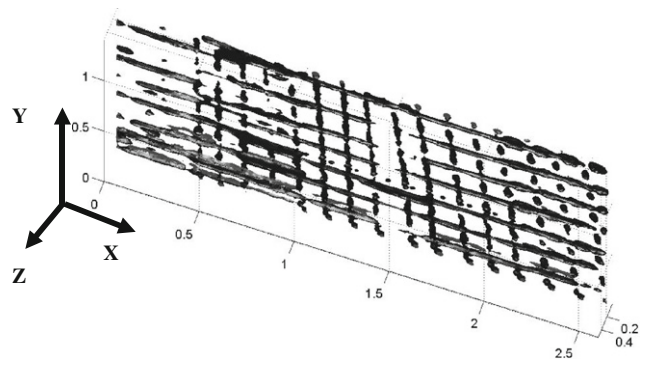


Fig. 17. Data cube, 0.0-0.5 m., inverse scattering and data fusion.

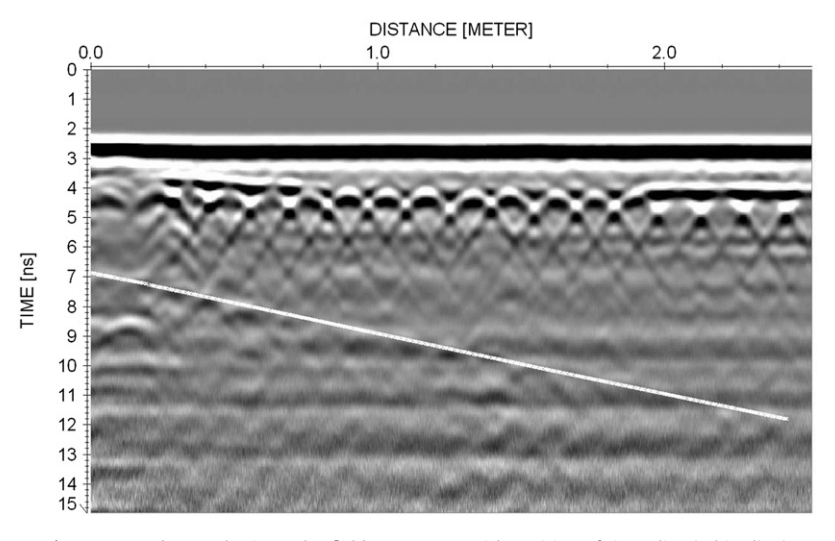


Fig. 18. Raw dataset, horizontal *E*-field, y=0.37 m, with position of time slice (white line).

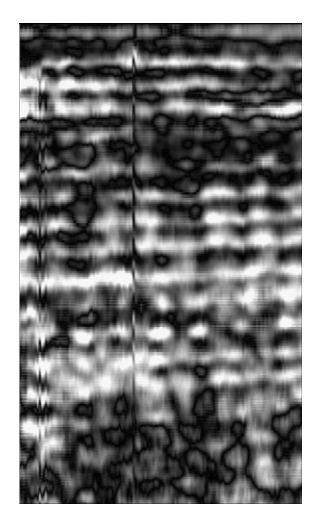


Fig. 19. time slice, 4.0-8.8 ns, 2-D processing.

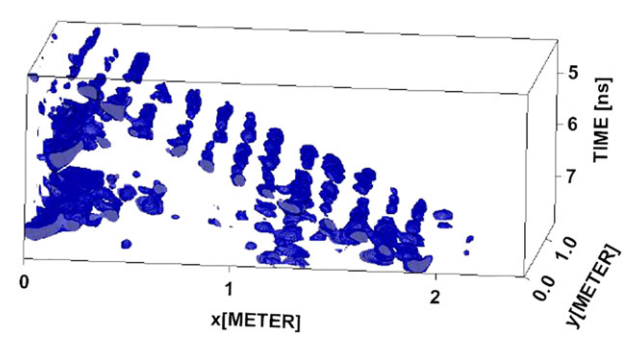


Fig. 20. Data cube 4.5-8.0 ns, 2-D processing.

evident. Accordingly, the rebar appears clearer and better focused and the reason for the increased reflection amplitudes visible in the top section of Fig. 14 becomes obvious.

4.2. Second layer of rebar

In Fig. 18 the raw dataset recorded with the horizontal E-field at position y=0.37 m is presented. The white line dipping from

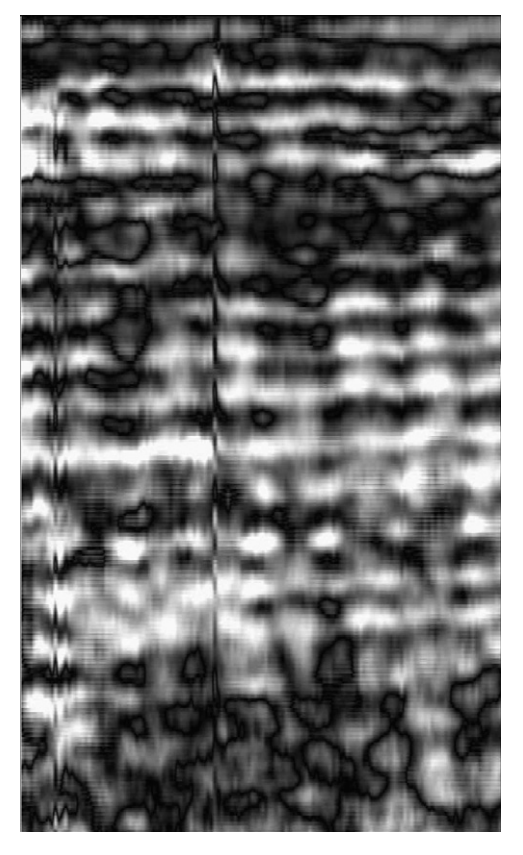


Fig. 21. Timeslice, 4.0–8.8 ns, 3-D processing and data fusion.

t=7.0 ns at x=0.00 m to t=11.8 ns at x=2.40 m shows the suspected position of a second layer of rebar (see also Figs. 5 and 9 for comparison). This suspected position shifts to t=4.0 ns at x=0.00 m and t=8.8 ns at x=2.40 m for the processed dataset because of the correction of the surface reflection/direct wave to time zero during 2-D processing. Plotting a time slice following this line using the data that were processed with the 2-D processing sequence results in Fig. 19. When comparing this time-slice to the time-slice showing the top layer of rebar (Fig. 12) it is obvious that resolution and focus have decreased. However, it is still possible to make out the horizontal bars of the second layer of rebar. This is confirmed by the presentation of the data cube in

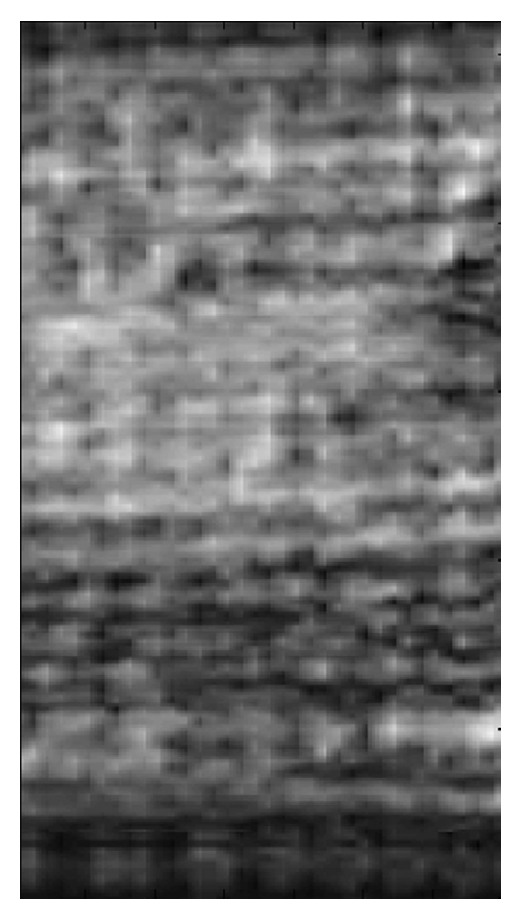


Fig. 22. Depth slice, 0.18-0.40 m, inverse scattering and data fusion.

Fig. 20 where, despite the presence of noise, the horizontal bars are clearly visible.

In Fig. 21 the time-slice after 3-D processing and data fusion corresponding to the dipping line in Fig. 18 is presented. When comparing this result with the result for the top layer it becomes obvious that the signal/noise ratio has decreased significantly. Both vertical and horizontal bars can be made out. In addition there is an increased response from the points where vertical and horizontal bars are crossing because of the constructive interference of the data from the two antenna orientations.

In Fig. 22 a depth a slice after inverse scattering and data fusion is shown for the second layer of rebar. Again, the signal/noise ratio has decreased significantly when compared to the result of the top layer (Fig. 16) but both horizontal and vertical bars can still be made out.

5. Summary and conclusions

A multi-sensor, multi-polarization dataset was acquired on a concrete retaining wall. The decay of higher amplitudes with increasing two-way travel time was demonstrated, thus characterizing the concrete structure as a low pass filter.

The dataset was processed using three different approaches: classical 2-D processing followed by the construction of a 3-D data cube, full 3-D processing followed by data fusion and inverse scattering followed by data fusion.

The 2-D processing using the data from one antenna only provided for the top layer of rebar a detailed mapping of the horizontal rebar and a low amplitude and low focus result for the vertical bars.

The 3-D processing followed by data fusion resulted in a complete map of both, horizontal and vertical rebars for the top layer of rebar.

The inverse scattering approach followed by data fusion provided for the top layer of rebar a complete map of both, horizontal and vertical rebars. In addition, the reason for increased reflection amplitudes in some areas was elucidated.

All three processing approaches produced a result of lower quality for the second layer of rebar. It is assumed this is mainly due to the fact that the concrete structure acts as a low pass filter for increased two-way travel time and because of the masking effect of the top layer of rebar. In other words, the result for the second layer of rebar shows rather the limits of the dataset than the limit of the different processing algorithms.

Acknowledgements

Special thanks to Roman Mastrangelo, formerly Empa, for his support during data acquisition and to the building department of the city of Duebendorf for providing the original building plans of the wall.

References

- [1] Hugenschmidt J., Mastrangelo R.. The inspection of large retaining walls using GPR. In: Proceedings of the fourtth international workshop on advanced ground penetrating radar, 27–29 June 2007, Naples, Italy, 2007. p. 267–71.
- [2] Hugenschmidt J, Kalogeropoulos A. The inspection of retaining walls using GPR. Journal of Applied Geophysics 2009;67:335–44.
- [3] Hugenschmidt: Multi-Offset-Analysis for man-made structures. In: GPR 2000, Proceedings of the eighth international conference on ground penetrating radar, 23–26 May 2000, Gold Coast, Australia, 2000. p. 414–20.
- [4] Kohl Ch., Krause M, Maierhofer Ch., Mayer K., Wöstmann J., Wiggenhauser H. 3D-visualisation of NDT-data using data fusion technique. In: Proceedings of the international symposium on destructive testing in civil engineering, 16–19 September 2003. Berlin, Germany, 2003.
- [5] Langenberg KJ, Mayer K, Marklein R. Nondestructive testing of concrete with electromagnetic and elastic waves; modeling and imaging. Cement & Concrete Composites 2006;28:370–83.
- [6] Capizzi P, Cosentino PL. GPR multi-component data analysisNear Surface Geophysics 2008;6:87–95.
- [7] Sbartai ZM, Viriyametanont K, Laurens S. NDE of reinforced concrete—inversion of GPR data using neural approach. In: Proceedings of the 12th international conference on ground penetrating radar, 16–19 June 2008, Birmingham. UK. 2008.
- [8] Soldovieri F, Prisco G, Hugenschmidt J. Microwave tomography for GPR diagnostics of reinforced concrete.In: Proceedings of the European microwave week 2009. September 28–October 2, Rome, Italy, 2009.
- [9] Solimene R, Soldovieri F, Prisco G, Pierri R. Three-dimensional microwave tomography by a 2-D slice-based reconstruction algorithm. IEEE Geoscience and Remote Sensing Letters 2007;4(4):556–60.
- [10] Soldovieri F, Persico R, Utsi E, Utsi V. The application of inverse scattering techniques with ground penetrating radar to the problem of rebar location in concrete. NDT&E International 2006;39:602–7.
- [11] Soldovieri F, Hugenschmidt J, Persico R, Leone G. A linear inverse scattering algorithm for realistic GPR applications. Near Surface Geophysics 2007;5(1): 29–42
- [12] Reflexw manual ver. 4.5 from 24.07.2007. Sandmeier scientific software, Karlsruhe, Germany.
- [13] Yilmaz Ö. Seismic Data Processing. Tulsa, USA: Society of Exploration Geophysicists; 1987.
- [14] Mallat S. A theory for multiresolution signal decomposition: the wavelet representation. IEEE Transaction. On Pattern Analysis and Machine Intelligence 1989;11(7):674–93.
- [15] Perrin S, Bibaut A, Duflos E, Vanheeghe P. Use of wavelets for ground-penetrating radar signal analysis and multisensor fusion in the frame of landmines detection. IEEE International Conference on Systems, Man, and Cybernetics 2000;4:2940-5.